*Protein Science* (1999), *8*:2406–2417. Cambridge University Press. Printed in the USA.


# Crystal structure of *Trypanosoma cruzi* tyrosine aminotransferase: Substrate specificity is influenced by cofactor binding mode

WULF BLANKENFELDT,[1] CRISTINA NOWICKI,[2] MARISA MONTEMARTINI-KALISZ,[1] HENRYK M. KALISZ,[1] AND HANS-JÜRGEN HECHT[1]

[1]Gesellschaft für Biotechnologische Forschung, Mascheroder Weg 1, D-38124 Braunschweig, Germany
[2]IQUIFIB (CONICET—Facultad de Farmacia y Bioquímica, Universidad de Buenos Aires), Junín 956, 1113 Buenos Aires, Argentina

(RECEIVED June 29, 1999; ACCEPTED September 2, 1999)

**Abstract**

The crystal structure of tyrosine aminotransferase (TAT) from the parasitic protozoan *Trypanosoma cruzi*, which belongs to the aminotransferase subfamily I$\gamma$, has been determined at 2.5 Å resolution with the *R*-value $R = 15.1\%$. *T. cruzi* TAT shares less than 15% sequence identity with aminotransferases of subfamily I$\alpha$ but shows only two larger topological differences to the aspartate aminotransferases (AspATs). First, TAT contains a loop protruding from the enzyme surface in the larger cofactor-binding domain, where the AspATs have a kinked $\alpha$-helix. Second, in the smaller substrate-binding domain, TAT has a four-stranded antiparallel $\beta$-sheet instead of the two-stranded $\beta$-sheet in the AspATs. The position of the aromatic ring of the pyridoxal-5′-phosphate cofactor is very similar to the AspATs but the phosphate group, in contrast, is closer to the substrate-binding site with one of its oxygen atoms pointing toward the substrate. Differences in substrate specificities of *T. cruzi* TAT and subfamily I$\alpha$ aminotransferases can be attributed by modeling of substrate complexes mainly to this different position of the cofactor-phosphate group. Absence of the arginine, which in the AspATs fixes the substrate side-chain carboxylate group by a salt bridge, contributes to the inability of *T. cruzi* TAT to transaminate acidic amino acids. The preference of TAT for tyrosine is probably related to the ability of Asn17 in TAT to form a hydrogen bond to the tyrosine side-chain hydroxyl group.

**Keywords:** Chagas' disease; pyridoxal-5′-phosphate; *Trypanosoma cruzi*; tyrosine aminotransferase; X-ray crystallography

Flagellated protozoa of the family *Trypanosomatidae* are among the most prevalent human pathogens, affecting more than 30 million people in tropical and subtropical areas (World Health Organisation, 1998). The diseases caused by these organisms include the American (also known as Chagas' disease) and African (sleeping sickness) trypanosomiasis, which are two distinct diseases caused by closely related parasites, *Trypanosoma cruzi* and *Thermus brucei*, respectively, and various forms of leishmaniasis caused by different species of *Leishmania*. All of these diseases are either debilitating or fatal. In all cases treatment is very difficult, with the currently available drugs being either highly toxic or of low efficacy, and no effective vaccines exist (World Health Organisation, 1998). There is therefore a need for the development of highly specific trypanocidal agents. One possible approach is to exploit the differences in the metabolic pathways of the parasites and the mammalian host.

One potential target for chemotherapeutic drug design may be the parasite amino acid metabolism, which involves aminotransferases with different substrate specificities to the mammalian enzymes. Although amino acid metabolism in the trypanosomatids is poorly understood, it is postulated to be involved in the cytosolic NADH reoxidation (Montemartini et al., 1994a, 1994b) and in methionine recycling (Berger et al., 1996, 1998). A high efficiency to transaminate aromatic amino acids has been described in some *Leishmania spp*. (Chatterjee & Ghosh, 1957; Fair & Krassner, 1971; Le Blanq & Lanham, 1984), *Crithidia fasciculata* (Constansas et al., 1971), *T. cruzi*, and *T. brucei* (Stibbs & Seed, 1975a). Additionally, at least the *T. cruzi* epimastigote form excretes aromatic amino acid catabolites into the culture media (Montemartini

Reprint requests to: Hans-Jürgen Hecht, Gesellschaft für Biotechnologische Forschung, Mascheroder Weg 1, Braunschweig, D-38124, Germany; e-mail: hjh@gbf.de, or Cristina Nowick, IQUIFIB, Junin 956, 1113 Buenos Aires, Argentina; e-mail: cnowicki@criba.edu.ar.

*Abbreviations:* AspAT, aspartate aminotransferase; PLP, pyridoxal-5′-phosphate; TAT, tyrosine aminotransferase.

et al., 1994a). Similar observations were made in animals infected by African trypanosomes, where high concentrations of aromatic lactates and pyruvates, as end products of the parasite amino acid catabolism, were detected in their urine (Stibbs & Seed, 1975b; El Sawalhy et al., 1998). The incidence of high levels of tyrosine aminotransferase (TAT) activity in the sera of mammals infected with African trypanosomes has been suggested as a diagnostic tool for the detection of early stages of parasitaemia (El Sawalhy & El-Sherbini, 1997). In mammals, in contrast, amino acid catabolism mainly takes place in the liver, where the carbon chains of most amino acids are oxidized in the Krebs cycle and their amino groups are converted to urea, which is ultimately excreted.

Aminotransferases (EC 2.6.1.x) are part of the $\alpha$-family of vitamin $B_6$-dependent enzymes (Alexander et al., 1994). On the basis of a comprehensive alignment, including sequence comparison, hydrophobicity patterns, and secondary structure prediction, Mehta et al. (1993) proposed that all of these enzymes most probably diverged from a common PLP ancestor gene, and identified four groups, whose members share similar functional properties. More recently, Jensen and Gu (1996) subdivided the superfamily of aminotransferase homologs into four families and identified seven subfamilies in family I aminotransferases.

The AspATs, which belong to subfamily I$\alpha$ in the nomenclature of Jensen and Gu (1996), are the most thoroughly studied enzymes of the aminotransferase superfamily. The cytosolic enzymes from higher vertebrates are highly specific toward their substrates L-aspartate, $\alpha$-ketoglutarate, L-glutamate, and oxaloacetate while the mitochondrial enzyme also has very low affinity for tyrosine (Miller & Litwack, 1971). Other AspATs from different prokaryotic sources are less specific as they can utilize several amino acids with different affinities (Kuramitsu et al., 1990) and some of them have been termed "broad substrate specificity aminotransferases" (Vernal et al., 1998).

Most of the crystal structures of aminotransferases determined to date belong to subfamily I$\alpha$. Crystallographic studies with the highly specific cytosolic and mitochondrial AspATs (Ford et al., 1980; McPhalen et al., 1992; Malashkevich et al., 1995b; Rhee et al., 1997) have disclosed the catalytic mechanism for dicarboxylic substrates (Kirsch et al., 1984). Recently, the structure of an aminotransferase from *Paracoccus denitrificans*, which uses aromatic as well as acidic amino acids as substrates has been reported (Okamoto et al., 1998), and its broad substrate spectrum attributed to the movement of some active site residues, especially Arg292, which was also observed in a hexamutant of *Escherichia coli* AspAT (Malashkevich et al., 1995a).

The subfamily I$\gamma$ enzymes presently are less well characterized, and no crystal structures have been reported to date. This subfamily contains diverse enzymes, including rat glucocorticoid inducible TAT (Grange & Pictet, 1985), human liver TAT (Rettenmeier et al., 1990), and TAT from *T. cruzi* (Montemartini et al., 1993, 1994a). While the mammalian TATs prefer tyrosine and $\alpha$-ketoglutarate as substrates (Iwasaki et al., 1973), the *T. cruzi* enzyme accepts three $\alpha$-ketoacids (pyruvate, $\alpha$-ketoglutarate, and oxaloacetate), all three aromatic amino acids and alanine as substrate with the best pairs being tyrosine-pyruvate and alanine-$\alpha$-ketoglutarate (Montemartini et al., 1993). TAT from *T. cruzi* is highly abundant, representing 3% of the total soluble protein with the *T. cruzi* genome containing approximately 70 TAT gene copies (Bontempi et al., 1993). The present three-dimensional (3D) structure determination of TAT from *T. cruzi* aims at structure-function relationship studies as a basis for drug design.

## Results and discussion

### *Overall structure*

The *T. cruzi* TAT dimer is an S-shaped molecule with dimensions of 100, 67, and 57 Å (Fig. 1). Superposition with the closed form of *E. coli* AspAT (Protein Data Bank (PDB) ID number 1ART; Okamoto et al., 1994), the structure used in molecular replacement, leads to the structure-based sequence alignment shown in Figure 2. From the insertion/deletion pattern, it can be clearly seen that *T. cruzi* TAT closely resembles human and rat TAT with sequence identities of 40.5%, while the recently published *P. denitrificans* aromatic aminotransferase (PDB ID number 1AY4; Okamoto et al., 1998) is more similar to the bacterial AspAT (sequence identity 45.5%). The sequence identity between *E. coli* AspAT and *T. cruzi* TAT is 13.0%.

The monomer of *T. cruzi* TAT exhibits a two-domain structure, like other aminotransferases (McPhalen et al., 1992). The larger of these domains contains the central part of the amino acid sequence and is dominated by a seven stranded mostly parallel $\beta$-sheet of the order 3245671 (strand 7 being antiparallel to the rest), which is flanked by helices on both of its faces. This $\alpha/\beta/\alpha$-sandwich architecture constitutes the cofactor-binding domain. This domain shows only minor topological changes to the I$\alpha$-AspATs, the largest ones being a stretch containing two $3_{10}$-helices between Lys99 and Asn106 ($\eta$1 and $\eta$2), which corresponds to an $\alpha$-helix in AspATs ($\alpha$4), and a loop protruding from the enzyme surface (Phe224 to Arg245) where the AspATs have a kinked $\alpha$-helix ($\alpha$9 and $\alpha$10). These two regions lie close to each other in the structure and therefore seem to be mutually stabilizing. They are also the only two regions in the protein's core where larger insertions/deletions are observed in comparison to the mammalian TATs. In addition to the two cis-prolines (Pro136 and Pro189), which are conserved in all family I aminotransferases, *T. cruzi* TAT has a third cis-proline at position 186, which is conserved in other aminotransferases of subfamily I$\gamma$.

The second, smaller, domain constitutes the substrate-binding domain. It consists of N- and C-terminal sequence regions and contains the highly conserved residue in family I for the binding of these enzymes' substrates, Arg389 in *T. cruzi* TAT, which fixes the $\alpha$-carboxylate of the incoming amino acid or $\alpha$-ketoacid. The topological differences to the I$\alpha$-aminotransferases are considerably larger in this part of the structure. Helix $\alpha$13 is shortened from 31 residues in *E. coli* AspAT to 22 in *T. cruzi* TAT and two insertions of ten and eight amino acids at positions 350 and 380, respectively, lead to a four-stranded antiparallel $\beta$-sheet in the parasite enzyme, instead of the two-stranded $\beta$-sheet in the enzymes from subfamily I$\alpha$.

The N-terminal residues Trp4 to Phe16 form an extended arm, separate from the two domains, which interacts with the larger domain of the second subunit. *T. cruzi* TAT has an additional short helix ($\alpha$0) in this region instead of an extended coil in the I$\alpha$-aminotransferases.

Although TAT contains 10 cysteine residues per subunit, the final structure model of *T. cruzi* TAT demonstrates, in accordance with chemical data (C. Nowicki, unpubl. results), the absence of disulfide bridges. Even the two cysteines located close to each other in the dimer interface (Cys292 from each subunit) do not form an interchain disulfide bridge, although a different side-chain rotamer would bring the sulfur atoms into a typical S-S-bond distance. This cysteine is conserved in mammalian TATs whose disulfide structure has not been investigated to date.

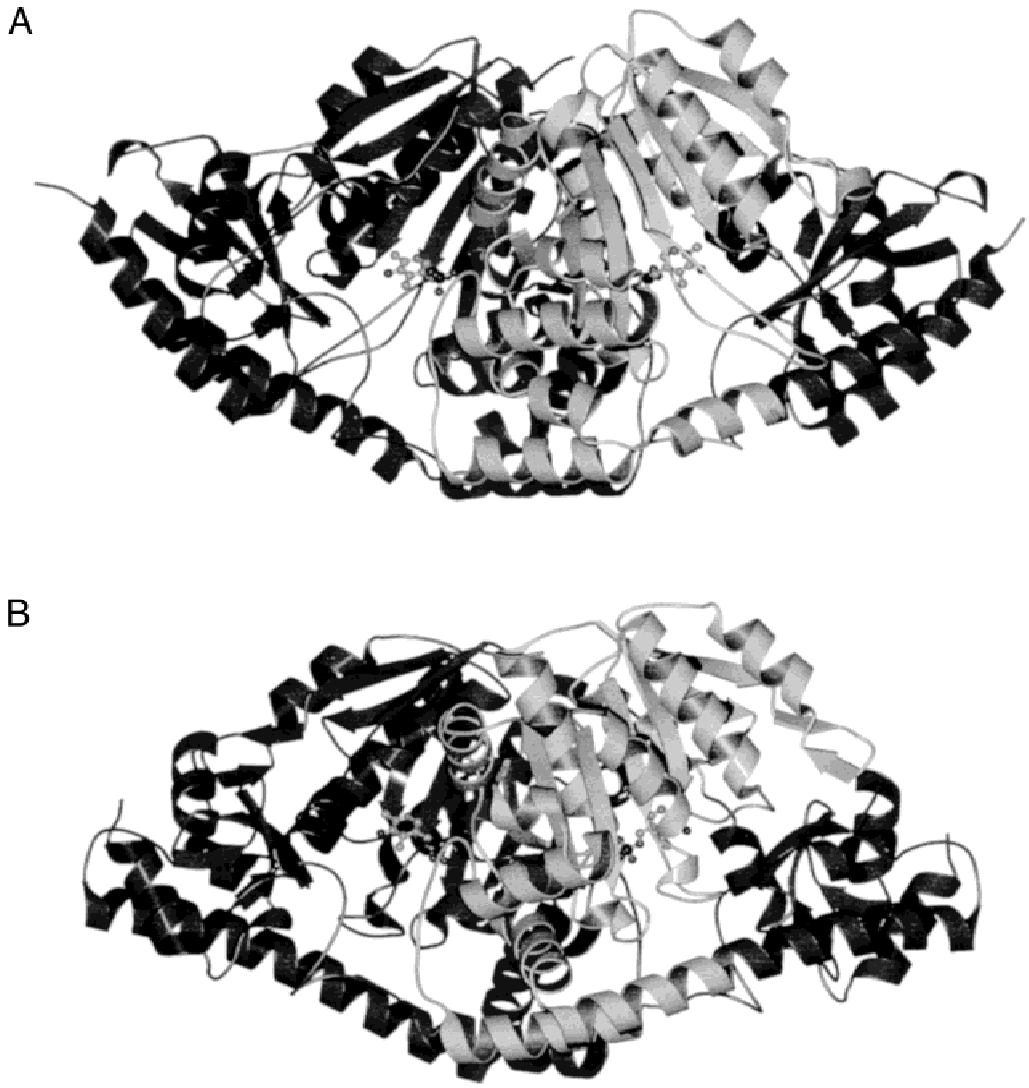


**Fig. 1.** Schematic representation of the (**A**) *T. cruzi* TAT and (**B**) *E. coli* AspAT dimer viewed along the substrate entry channel of one subunit, perpendicular to the twofold axis. The domain organization is indicated for one of the subunits (bright grey, N-terminal arm; dark, substrate-binding domain; bright, cofactor-binding domain). PLP is shown as a ball and stick model.

*The active center of T. cruzi TAT*

The key residues involved in cofactor and substrate binding in other aminotransferases are conserved in the active center of *T. cruzi* TAT (Fig. 3A,B). PLP forms a Schiff base with Lys253, with the double bond being almost perpendicular to the pyridine ring of the cofactor. This indicates that this internal aldimine bond has a p$K_a$ value lower than the pH 7.0 of the crystallization buffer and is not protonated in the present structure (Hayashi et al., 1998). Moreover, Lys253 exhibits an unusually small $\chi 4$ torsion angle of 4° in a side-chain conformation similar to *E. coli* phosphoserine aminotransferase (PDB ID number 1BT4), an enzyme belonging to the aminotransferase family IV (Hester et al., 1999). This strained conformation may destabilize the internal aldimine and enhance the reactivity of the enzyme with the amino acid substrate (Fig. 3C).

The orientation of the aromatic ring of PLP in *T. cruzi* TAT is determined by numerous polar and nonpolar interactions and is very similar to other aminotransferases from subfamily I$\alpha$. Its nitrogen atom N1 is hydrogen bonded to Asp216, an absolutely conserved residue in the aminotransferase superfamily. This PLP-N1/D216-O$\delta$2 hydrogen bond ensures that the nitrogen atom remains protonated during the whole transamination reaction and with its stabilized positive charge enhances the cofactor's role as "electron sink" (Fig. 4) (Yano et al., 1992). Asp216 is stabilized in *T. cruzi* TAT by hydrogen bonds to Tyr141 on helix $\alpha$6 and Thr184 on strand $\beta$4. It is probably stabilized similarly in mammalian TATs, where threonine is replaced by asparagine, while in *E. coli* AspAT, and in other AspATs, His143 on helix $\alpha$6 and Ser139 on the loop ensuing strand $\beta$2 are involved. PLP's phenolic oxygen is deprotonated and forms strong hydrogen bonds to the absolutely conserved Asn188 N$\delta$2 ($d$ = 2.6 Å) and to Tyr219 O$\eta$ ($d$ = 2.5 Å), which is replaced by phenylalanine in only a very few sequences. These interactions prevent rotation of the pyridinium ring, which would enable the formation of a hydrogen bond between the phe-

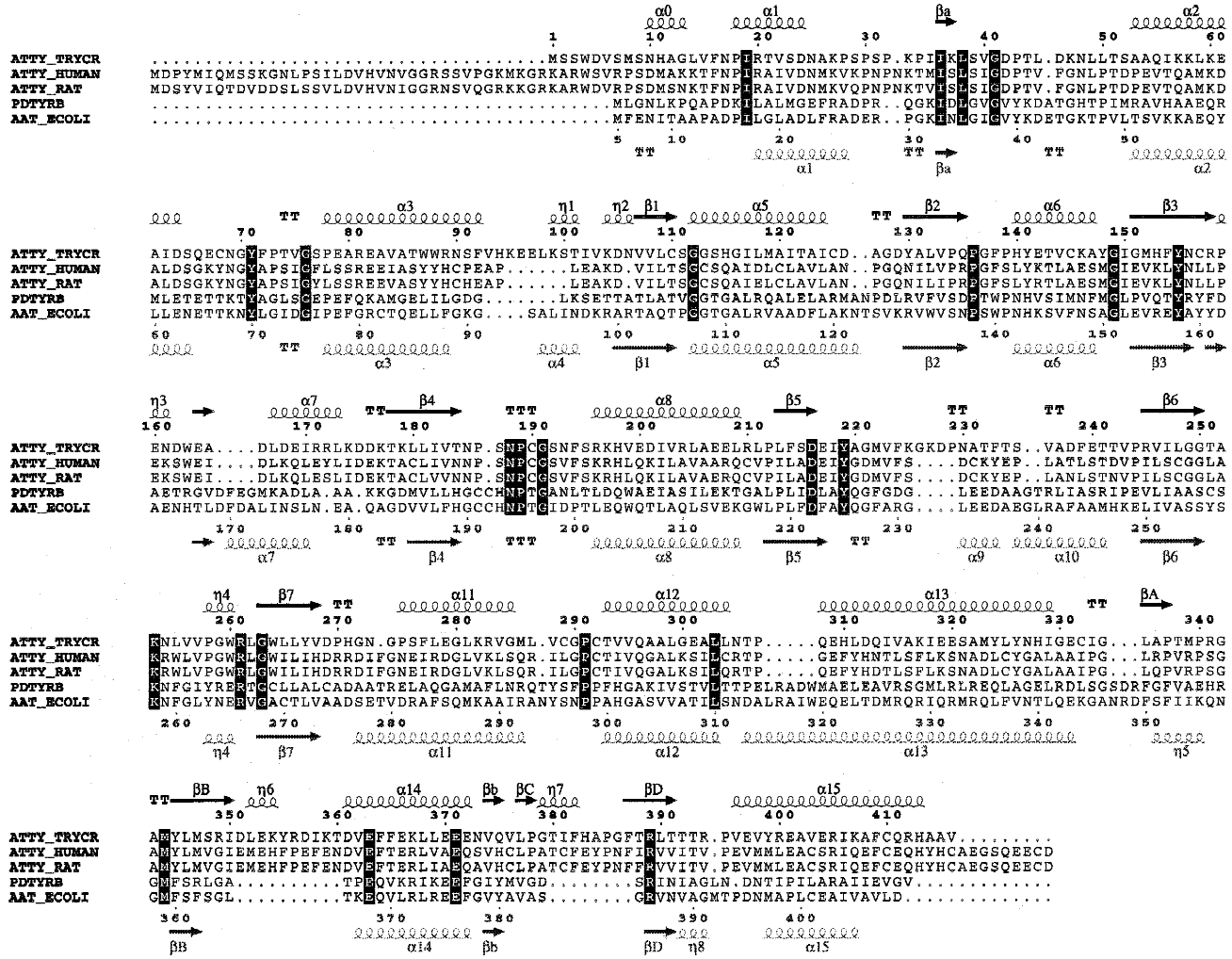


**Fig. 2.** Structure-based sequence alignment of *T. cruzi* TAT (ATTY_TRYCR) and *E. coli* AspAT (AAT_ECOLI). Human (ATTY_HUMAN) and rat TAT (ATTY_RAT) were conventionally aligned to *T. cruzi* TAT as was *P. denitrificans* aromatic aminotransferase (PDTYRB) to *E. coli* AspAT. The secondary structures of *T. cruzi* TAT and *E. coli* AspAT are shown in black and grey, respectively. Conserved residues are highlighted.

nolic oxygen and the nitrogen of the Schiff base. This hydrogen bond would increase the internal aldimine's p$K_a$ (Hayashi et al., 1998) and would thus hinder deprotonation of the incoming zwitterionic amino acid in the first reaction step (Fig. 4). Both Asn188 and Tyr219 are stabilized further by hydrogen bonds to Tyr345. Tyr345 is also found in mammalian TATs but not in the AspATs from subfamily I$\alpha$ where a phenylalanine occupies the equivalent position (Fig. 3A,B). The cofactor's aromatic ring is fixed further by a stacking interaction with Phe138 and a contact with C$\delta$2 of Ile218 (Fig. 3C), which occupies the same position as C$\beta$ of the corresponding Ala224 in *E. coli* AspAT. In the I$\alpha$-aminotransferases, Trp140 occupies the position of Phe138, where it is used to fix the enzyme-bound aspartate by a hydrogen bond between N$\epsilon$1 and the $\beta$-carboxylate group (Okamoto et al., 1994, 1998).

Several interactions positioning the PLP's phosphate group are preserved, including the salt bridge between phosphate and Arg261, the interaction with the dipole generated by helix $\alpha$5, the two hydrogen bonds to OH, and the backbone nitrogen of Ser114, and the hydrogen bond to the side chain of Tyr71* from the second subunit. However, substitutions of hydrophilic residues by hydrophobic residues at positions 250 and 252 in *T. cruzi* and mammalian TATs, which have glycine and alanine in these positions, remove additional hydrogen bonds fixing the phosphate, which are formed in the bacterial AspAT with the side chains of Ser255 and Ser257. In their place a network of four water molecules links the oxygens of the phosphate group to the backbone of the protein in the parasite enzyme. All of these water molecules have a temperature factor well below average but a misinterpretation of ion binding seems to be ruled out by the binding distances (2.6–3.3 Å) and the absence of residual electron density. The water molecule closest to the cofactor is bound most tightly ($B$ = 5.0 Å$^2$) and occupies the position of one of the phosphate's oxygen atoms in the AspATs from subfamily I$\alpha$. The cofactor in *T. cruzi* TAT therefore shows different torsion angles ($\phi = -87°$ and $\psi = 147°$, for definition see Fig. 4) than in the other two enzymes in their open forms ($\phi = -15°$ and $\psi = -177°$). Consequently, the phosphate group of

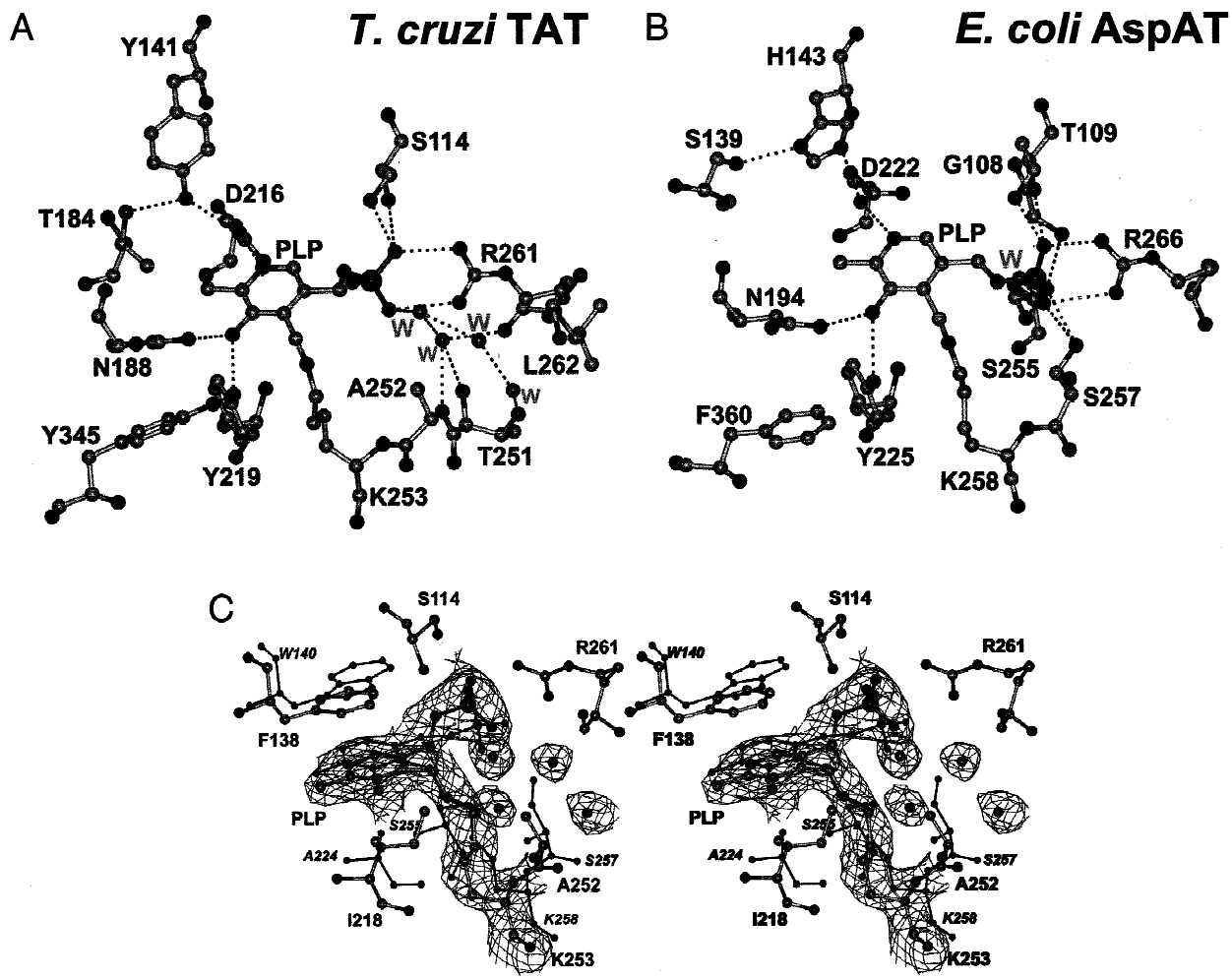


**Fig. 3.** Hydrogen bonding networks in the active centers of (**A**) *T. cruzi* TAT and (**B**) *E. coli* AspAT. Tyr71*/Tyr70* have been omitted for clarity. (**C**) Stereoplot of $\sigma_A$-weighted $2F_o - F_c$ electron density of the PLP/Lys253 Schiff base and the four associated water molecules in the active centre of *T. cruzi* TAT, contoured at $1.25\sigma$. Selected residues of *E. coli* AspAT are overlaid in dark thin lines (Okamoto et al., 1994).

*T. cruzi* TAT is closer to the active site and one of its oxygen atoms points toward rather than away from the substrate-binding site. The current model has no interaction partner for this oxygen atom although weak residual difference electron density might indicate the presence of three weakly bound water molecules in hydrogen bonding distance.

Repositioning of the phosphate group to the coordinates found in subfamily I$\alpha$ would not only require expulsion of the most tightly bound water molecule, but would also force the negative charge of phosphate close to the hydrophobic side chains of Ala252 and Ile218, whose C$\delta$1 occupies the position of C$\beta$ of Ser255 in *E. coli* AspAT. Therefore, it seems highly unlikely that the position of the PLP phosphate group can change in *T. cruzi* TAT to a position similar to the enzymes from subfamily I$\alpha$

In the current conformation the charged phosphate group generates a negative potential near the cofactor's aldimine carbon atom C4A where the substrate attacks through its $\alpha$-amino group. As this group is likely to be protonated initially, the phosphate group in *T. cruzi* TAT probably directs the incoming substrate toward the reaction center.

*Substrate binding and specificity of T. cruzi TAT*

TAT reacts efficiently with all aromatic amino acids, with tyrosine being the preferred substrate as demonstrated by the apparent kinetic constants (Montemartini et al., 1993). The enzyme also has a similar affinity for alanine (Montemartini et al., 1993) and methionine (C. Nowicki, unpubl. results). In contrast, aspartate cannot be used (Nowicki et al., 1992) and branched amino acids, such as leucine, isoleucine, and valine are poor substrates (C. Nowicki, unpubl. results).

In the second half-reaction the great majority of aminotransferases, including the mammalian TATs (Iwasaki et al., 1973; Andersson & Pispa, 1982), use $\alpha$-ketoglutarate as the preferred substrate, and the glutamate formed is normally reoxidized by a specific NADH-dependent glutamate dehydrogenase. Thus, $\alpha$-ketoglutarate acts as a shuttle compound in amino acid catabolism. TAT from *T. cruzi*, in contrast, prefers the smaller pyruvate to the dicarboxylic molecules $\alpha$-ketoglutarate and oxaloacetate (Montemartini et al., 1993). This property corresponds to the inability of the enzyme to use aspartic acid as substrate and may reflect that

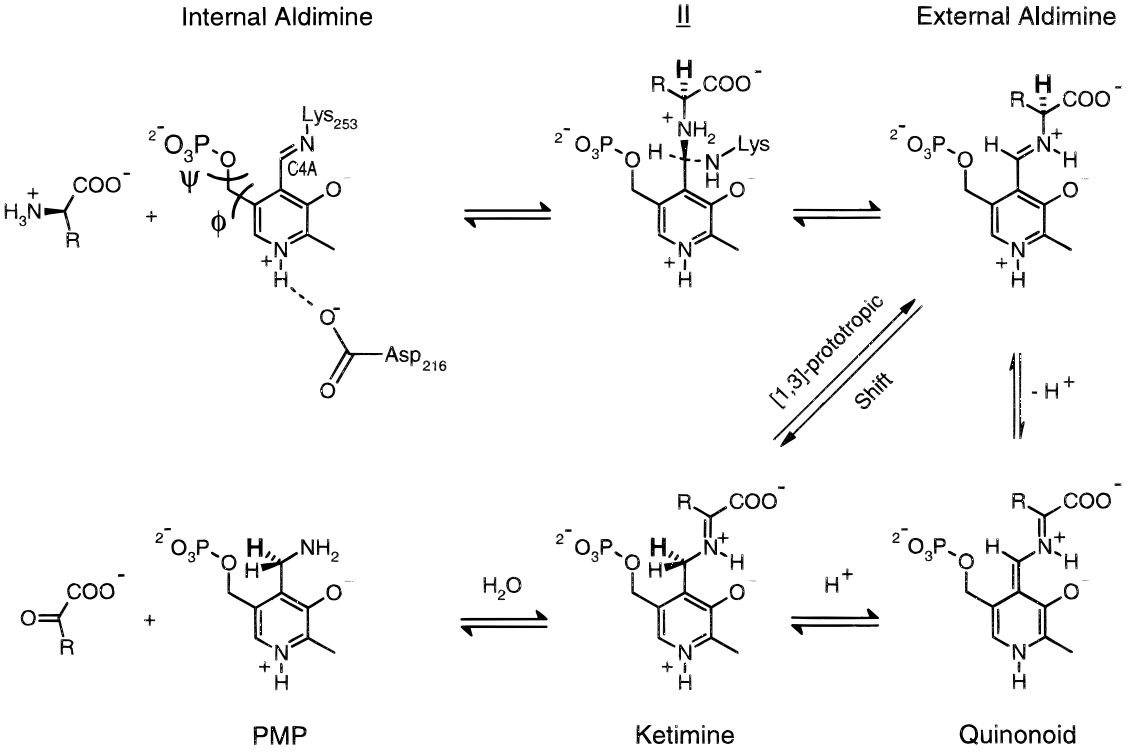


**Fig. 4.** Mechanism of the enzymatic transamination reaction according to Kirsch et al. (1984). The torsion angles $\phi$ and $\psi$ as well as the C4A atom of the cofactor are indicated. The reaction proceeds via the geminal diamine II to an external aldimine, which is subsequently deprotonated at the C$\alpha$ of the amino acid substrate. Reprotonation at C4A leads to a ketimine, which is then hydrolyzed to the cofactor in its pyridoxamine-5′-phosphate form (PMP) and to formation of the corresponding $\alpha$-ketoacid. The transferred hydrogen atom is in bold.

*T. cruzi* TAT fulfills a different physiological role from the mammalian TAT as the parasite's metabolism lacks the urea cycle (Cazzulo, 1992). In the related trypanosomatids *C. fasciculata* and *T. brucei brucei*, Berger et al. (1996) found that aromatic amino acids are used in the regeneration of methionine from $\alpha$-ketomethiobutyrate, which probably links TAT to the synthesis of polyamines. However, the *C. fasciculata* enzyme shows only 10% of the activity with pyruvate in comparison to $\alpha$-ketoglutarate (Rege, 1987) and differs at least in this aspect from *T. cruzi* TAT.

As attempts to obtain crystals of an enzyme-inhibitor complex were unsuccessful, molecular modeling of inhibitor binding based on aminotransferase-inhibitor structures from the PDB as well as docking simulations with substrate molecules were carried out. They show that the natural aromatic amino acids fit easily and in the correct orientation in the active center of *T. cruzi* TAT (Fig. 5A–C). The carboxylate group of the incoming amino acid forms a salt bridge with Arg389, and hydrogen bonds are formed between the oxygen atom distal to the cofactor and the backbone nitrogen of Gly41 and between the proximal oxygen and N$\delta$2 of the conserved Asn188. The $\alpha$-amino group in these complexes is in hydrogen bonding distance to O$\eta$ of Tyr345 and to the carbonyl oxygen of Gly41 (both distances are 2.8 Å for tyrosine) and is positioned approximately in the plane of the cofactor's pyridinium ring between PLP's phenolic oxygen and the reactive C4A (Fig. 5B).

The simulations suggest that tyrosine, in contrast to phenylalanine and tryptophan, can form an additional hydrogen bond between its phenolic OH and N$\delta$2 of Asn17. This potential interaction leads to a remarkable reproducibility of the position of the amino acid's side chain in the simulations while other substrates give an impression of high side-chain flexibility due to only unspecific interactions with the protein. Asn17 lies in the small substrate-binding domain and could therefore guide tyrosine closer toward the reaction center in the course of domain closure. However, both the $\varphi$ and the $\chi$1 torsion angles of the tyrosine substrate would have to change considerably if the hydrogen bond with Asn17 is to be preserved during the reaction. The enzymatic transamination requires movement of the bond between C$\alpha$ and H$\alpha$ into an orientation perpendicular to the external aldimine bond, which in turn has to be positioned coplanar to the cofactor's aromatic ring for maximum delocalization of the emerging negative charge at C$\alpha$ (Fig. 4). It has to be kept in mind, therefore, that the docking simulations do not take into account conformational changes of the complex required to reduce the distance between the docked $\alpha$-amino group and the reactive C4A (3.7 Å), such as tilting of the cofactor's aromatic ring or a domain movement similar to that seen in other aminotransferases and also likely to occur in *T. cruzi* TAT. The complexes shown in Figure 5 may therefore be regarded as Michaelis adducts.

Aspartate and glutamate show deviating behavior in the simulations. As the second arginine of the second subunit, which is used by the AspATs for the orientation of these substrates (Arg292* in *E. coli* AspAT), is missing in *T. cruzi* TAT, the simulations preferentially dock these amino acids "upside-down" (Fig. 5D), preventing the transamination reaction as the $\alpha$-hydrogen atom is not facing Lys253.

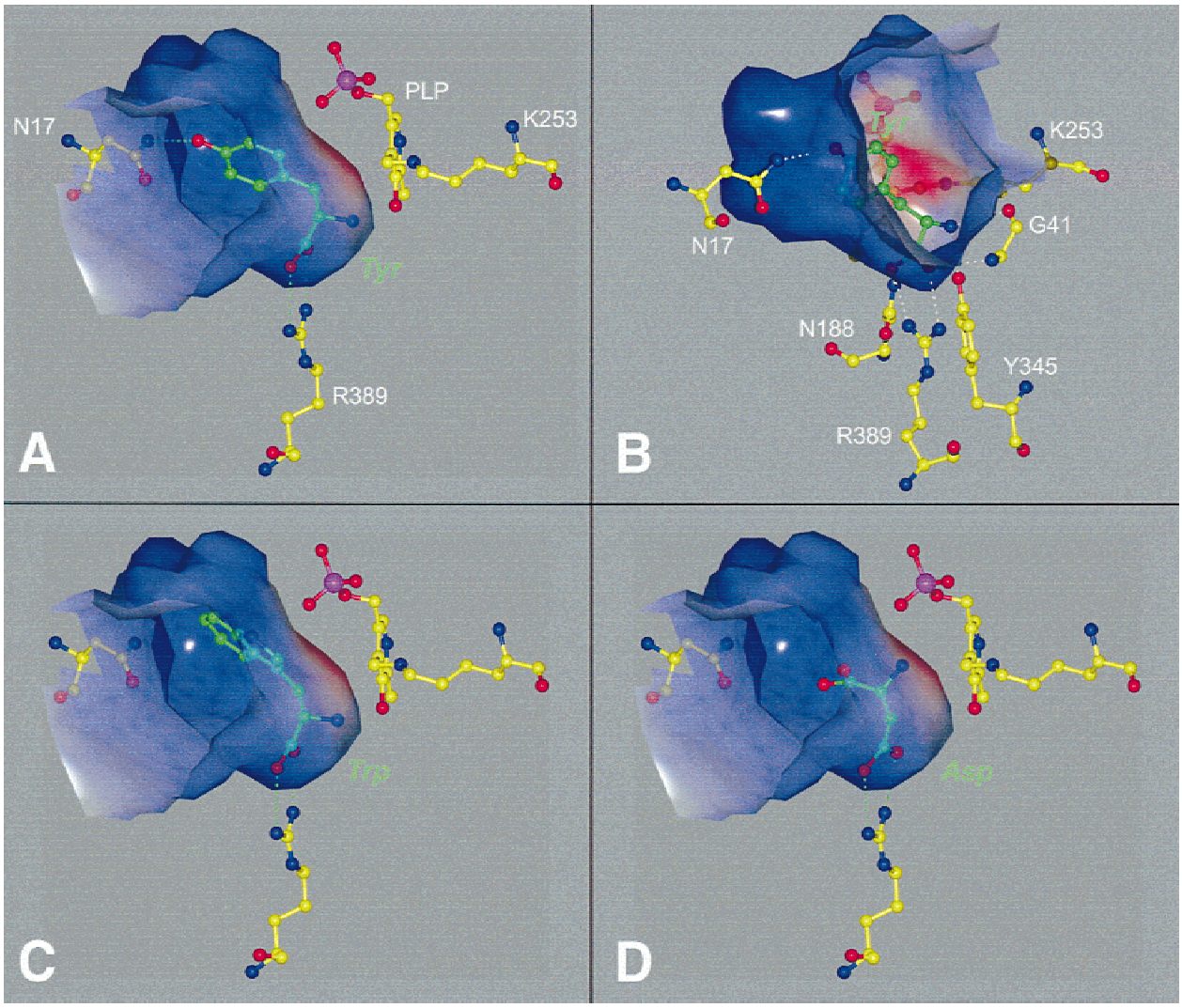


**Fig. 5.** Active site pocket of *T. cruzi* TAT, colored by surface potential, showing two different perspectives of (**A, B**) docked tyrosine, and (**C**) the positions of docked tryptophan, and (**D**) docked aspartic acid.

Modeling the external aldimine intermediate analogous to the published methylaspartate inhibitor complex of *E. coli* AspAT (Okamoto et al., 1994) provides an additional explanation for the inability of *T. cruzi* TAT to use aspartic acid as substrate. In this model the $\beta$-carboxylate group of aspartate would be very close to the cofactor's phosphate group (Fig. 6), causing a strong repulsive force due to the accumulation of negative charges. This unfavorable interaction cannot be avoided easily as rotation of the side chain around $\chi 1$ would cause another repulsive contact with the substrate's own $\alpha$-carboxylate group or would lead to steric clashes with residues Gly41 and Tyr71* of the second subunit. Repositioning of the phosphate group during substrate binding, on the other hand, is not possible as the phosphate is fixed in an extended network of polar interactions (Fig. 3A) and has an anchor like function in related aminotransferases, forming together with the methyl group of the cofactor the end point of a rotation axis for the pyridinium ring (Kirsch et al., 1984). A similar situation will arise with glutamate, which has an additional torsion angle to escape the phosphate group but needs even more space. As the reverse reaction proceeds through the same external aldimine, the phosphate binding mode of *T. cruzi* TAT also explains the preference of pyruvate over the dicarboxylic $\alpha$-ketoacids in the second half of the transamination cycle.

Other substrates whose side chains extend beyond a C$\beta$ may also interact with the phosphate group. Rearrangement of the side chains to prevent steric clashes with the phosphate anchor is particularly difficult with the branched residues valine, leucine, and isoleucine, which are poor substrates (C. Nowicki, unpubl. results), and might explain why the lowest apparent $K_m$-value has been observed with alanine.

### *A preliminary glimpse into the structure of mammalian TAT*

*T. cruzi* and mammalian TATs share a sequence identity of 40.5%. Of the mammalian TATs, only the rat liver enzyme has been characterized enzymatically to some extent (Iwasaki et al., 1973; Dietrich et al., 1991), but its high sequence identity of more than 90% implies that human liver TAT possesses very similar properties.

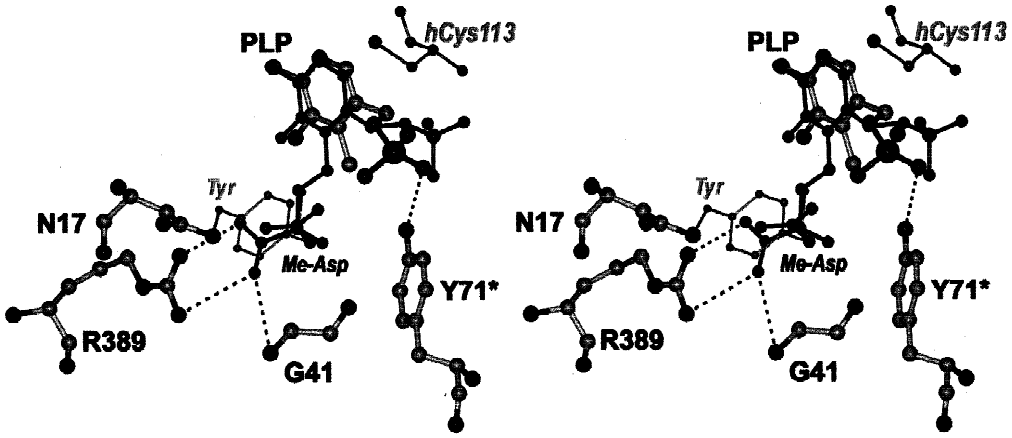


**Fig. 6.** Stereoplot of an external aldimine of tyrosine (grey) modeled in the active centre of *T. cruzi* TAT. $\alpha$-Methylaspartyl-PLP from complexed *E. coli* AspAT (Okamoto et al., 1994) is overlayed in dark lines (Me-Asp). The hypothetical position of a cysteine in the active center of human TAT is indicated (hCys113).

Alignment of the *T. cruzi* and mammalian TAT sequences (Fig. 2) shows only two larger insertions of six and four residues and three single residue insertions/deletions, thus implying reasonably close structural similarity of the three enzymes.

Mutations in the human TAT gene can lead to an inherited enzyme deficiency causing tyrosinaemia type II, also known as Richner–Hanhart syndrome (Richner, 1938; Hanhart, 1947; Fellman et al., 1969). Most of the mutations identified to date are nonsense mutations that lead to an incomplete protein (Natt et al., 1992; Hühn et al., 1998). The effect of the few characterized point mutations (Hühn et al., 1998) can readily be explained from the structure template. The exchange of Arg81 for a tryptophan (position 119 in human TAT; Hühn et al., 1998) places a residue with a high spatial requirement at the top of helix $\alpha$3. It is not possible to fit this tryptophan in any favorable rotamer without steric clashes with the backbone of the protein structure. The mutation should therefore lead to a misfolded protein. Substituting a hydrophobic amino acid with an arginine at position 170 (L201R mutation in human TAT; Hühn et al., 1998) places a positive charge in the middle of an extensive hydrophobic cluster consisting of at least 10 residues in the mammalian enzyme. As the side chain of arginine cannot be arranged to avoid clashes with other atoms, this mutated protein is also likely to be misfolded.

Reduced TAT activity was found in mutations affecting Arg405 (R433Q and R433W in human TAT; Hühn et al., 1998). The guanidinium group of this amino acid is involved in a hydrogen bonding network with the carbonyl oxygen of Glu372, with Glu401 O$\epsilon$2 and with the carbonyl oxygen of residue 34 in the substrate-binding domain. Although not all of these residues are conserved in human TAT, the hydrogen-bonding network should be similar due to the conservation of Glu372 and the close structural relationship of the TATs. The reduced activity of these mutants may therefore be caused by a distortion of this hydrogen bonding network and its influences on the substrate-binding domain.

A more complicated situation arises in a genetic variant having a splice mutation of unknown consequence and a potential substitution of glycine for valine at position 334 (362 in human TAT; Natt et al., 1992). This glycine is conserved in mammalian TATs and is located in a loop at the C-terminus of helix $\alpha$13. It has a backbone conformation that cannot be adopted easily by other amino acids ($\varphi = 87°$; $\psi = -4°$) and a mutation at this position may cause misfolding. However, as this residue is located far from the active center, the possibility cannot be ruled out that the observed pathological condition is caused by nonsense mutations resulting from a change in the splicing site.

Mammalian TATs differ from *T. cruzi* TAT in their preference of $\alpha$-ketoglutarate over pyruvate. Moreover, they have a more pronounced specificity for tyrosine than *T. cruzi* TAT and cannot accept alanine as a substrate (Dietrich et al., 1991). Modeling shows that all of the amino acids forming the active center of *T. cruzi* TAT are retained in rat and human TAT with the exception of residue 113 where glycine is replaced by cysteine. The G113C substitution would cause steric clashes should the PLP of the mammalian TATs be positioned in the same way as in *T. cruzi* TAT (Fig. 6). However, the deletions between residues 94 and 101 and/or at 106 may shift helix $\alpha$5 relative to the rest of the active center, thereby creating the space required by the phosphate group to occupy a similar position as in *T. cruzi* TAT. The substitution of hydrophobic residues for the phosphate-binding serine residues of the AspATs seems to indicate this. Hence, the preference of rat and human TATs for dicarboxylic $\alpha$-ketoacids instead of pyruvate would also have to be the consequence of structural changes in the region 104 to 113. As Cys113 seems to be the only accessible cysteine in the active center of the mammalian TAT model, it is tempting to speculate that this residue is responsible for the $\gamma$-cystathionase-catalyzed reversible deactivation of these enzymes by cystine-derived thiocysteine or free sulfur (Hargrove & Wichman, 1987; Hargrove, 1988).

### *T. cruzi TAT as a potential drug target*

For an enzyme to be useful as a drug target, it has to be of vital importance for the pathogenic organism and its inhibition must not evoke disproportional side effects in the host. If related enzymes exist in both the host and the pathogen, the chances of selecting a potential drug target are higher the more the enzymes differ structurally and functionally.

Mammalian TATs are hepatic glucocorticoid-inducible proteins that catalyze the first step in tyrosine catabolism. Their inherited depletion in humans causes the autosomal recessive disorder

Richner–Hanhart syndrome, a disease whose symptoms can be alleviated by administering a low-tyrosine/low-phenylalanine diet (Hunziker, 1980).

The role of TAT in *T. cruzi*, on the other hand, is a matter of ongoing debate. High concentrations of the enzyme in the epimastigotes of *T. cruzi* indicate that its function may be crucial for the parasite. TAT has been implicated in energy metabolism (Montemartini et al., 1994a), with aromatic amino acid catabolism and glycolysis being interrelated (Cazzulo et al., 1985). The glycolytic process in trypanosomatids presents some distinctive characteristics compared to the mammalian host (Opperdoes, 1987): (1) in the glycosome, a specialized organelle, glucose is converted to 1,3-diphosphoglycerate, which is released into the cytosol and subsequently metabolised to pyruvate; (2) hexokinase and phosphofructokinase are unregulated by glycolytic effectors such as fructose 2,6-bisphosphate but pyruvate kinase, in contrast, is strongly activated in the cytosol by fructose 2,6-bisphosphate leading to the production of large amounts of pyruvate; (3) the tricarboxylic cycle and the respiratory chain are much less efficient than in mammals; (4) cytosolic pyruvate is transaminated with the aromatic amino acids in a reaction involving TAT with L-alanine being one of the major metabolic end products of glycolysis, which is excreted in high concentrations into the culture media. The corresponding $\alpha$-ketoacids formed during this transamination reaction are reduced to aromatic lactates by an aromatic $\alpha$-hydroxy acid dehydrogenase leading to cytosolic NADH reoxidation and to the excretion of aromatic lactates into the culture media (Montemartini et al., 1994a, 1994b). Both reactions may constitute one of several ways, in addition to the tricarboxylic cycle, the parasite possesses for NADH regeneration (for review, see Cazzulo et al., 1985).

Trypanosomal TAT has also been postulated to play a role in polyamine synthesis, with aromatic amino acids being the prefered amino donors for the transamination of $\alpha$-ketomethiobutyric acid to methionine in *T. brucei* and *C. fasciculata* (Berger et al., 1996, 1998). In trypanosomatids condensation of the polyamine spermidine with glutathione leads to the formation of trypanothione, a reducing agent which mediates peroxide detoxification in *C. fasciculata* and probably other trypanosomatids (Nogoceke et al., 1997). Trypanothione has, to date, only been detected in trypanosomatids and a few other parasitic protozoa, and all enzymes involved in its biosynthesis might therefore represent targets of high value in the eradication of these parasites (Flohé, 1998). However, the presence of a mammalian host TAT with a sequence homology of approximately 50% to the parasite's enzyme must be of high concern should *T. cruzi* TAT be selected as a drug target since side effects of an artificial tyrosinaemia type II have to be avoided.

## Materials and methods

### *Crystallization, data collection, and processing*

TAT from *T. cruzi* epimastigotes was purified and crystallized as described previously (Montemartini et al., 1993; Nowicki et al., 1998). Two native diffraction data sets were used for the refinement. Data set 1 was collected from a single flash cooled crystal on beamline BW6 at the Deutsches Elektronen Synchrotron (DESY) in Hamburg with a wavelength of 1.1 Å, using a MAR imaging plate and the programs DENZO and SCALEPACK (Otwinowski, 1993) for data processing. The crystal was taken from a sitting drop that had been equilibrated against 25% (w/w) PEG 4000, 0.1 M citrate/phosphate buffer, pH 6.7. Cooling was achieved by shortly washing the crystal in cryoprotectant solution (30% (w/w) PEG 4000, 15% (v/v) glycerol, 0.1 M citrate/phosphate buffer, pH 7.4) prior to transfer into a nitrogen gas stream at 100 K. Data set 2 was measured at 285 K from five crystals that were grown by dialysis against 25% (w/w) PEG 8000, 5 mM PLP buffered at pH 7.0 with 0.1 M citrate/phosphate. These data were determined on a Siemens rotating copper anode equipped with an X1000 multiwire area detector. Indexing and integration were done with the X-gen module of the Cerius$^2$ software (Biosym/MSI, 1996), followed by scaling and data reduction with SCALA (Evans, 1997) and AGROVATA (CCP4, 1994). Both datasets belong to the space group $P2_1$ with similar lattice constants (data set 1: $a = 59.8$ Å, $b = 102.0$ Å, $c = 77.8$ Å, $\beta = 110.2°$; data set 2: $a = 61.6$ Å, $b = 102.2$ Å, $c = 77.9$ Å, $\beta = 110.3°$) and reveal an equivalent signal for one noncrystallographic twofold axis in their self-rotation functions (calculated with REPLACE; Tong & Rossmann, 1990), indicating the presence of one dimer per asymmetric unit. Data collection statistics are given in Table 1.

### *Refinement*

The structure of *T. cruzi* TAT was solved by molecular replacement with the program AMoRe (Navaza, 1994), using the coordinates of the closed form of *E. coli* AspAT (PDB ID number 1ART; Okamoto et al., 1994) as a search model. The correct rotation function solution was identified by comparison with the self-rotation function of the native datasets. To find the position of the rotated molecule in the unit cell, the search model had to be reduced to a polyalanine sequence for the nonconserved residues and it was only with dataset 1 that a reasonable solution without crystal packing conflicts could be obtained (resolution for translation search and rigid body refinement: 15–5 Å, Patterson integration limits: 0–42 Å; correlation coefficient highest/second highest peak: 45/42.3; *R*-value highest/second highest peak: 52.3/52.4). The refine-

**Table 1.** *Data collection statistics*

| Dataset | 1[a] | 2 |
|---|---|---|
| Space group | $P2_1$ | $P2_1$ |
| Unit-cell parameters | | |
| $a$ (Å) | 60.2 | 61.6 |
| $b$ (Å) | 102.3 | 102.2 |
| $c$ (Å) | 78.1 | 77.9 |
| $\beta$ (deg) | 110.2 | 110.3 |
| Resolution range | 41.9–2.30 Å | 10.0–2.51 Å |
| No. of unique reflections | 36,866 | 24,668 |
| $R_{merge}$[b] | | |
| Overall (%) | 6.7 | 5.1 |
| Last shell (%) | 14.3 (2.40–2.30 Å) | 9.6 (2.64–2.51 Å) |
| Completeness | | |
| Overall | 93.3 | 78.4 |
| Last shell | 88.4 (2.40–2.30 Å) | 47.0 (2.66–2.51 Å) |
| $\langle I/\sigma(I)\rangle$ | | |
| Overall | 13.0 | 17.0 |
| Last shell | 6.4 (2.40–2.30 Å) | 6.0 (2.61–2.51 Å) |
| Redundancy | 1.9 | 1.7 |

[a] Only data to 3.0 Å have been used in the refinement (see text).
[b] Merging *R*-factor; $R_{merge} = \sum|I_i - \langle I\rangle|/\sum I_i$.

ment was started with the complete model of *E. coli* AspAT against dataset 1 (resolution limit 3.0 Å), applying strict noncrystallographic symmetry and a bulk solvent model in the programm X-PLOR 3.851 (Brünger, 1992). In each stage of the refinement, multiple runs of conventional (Brünger et al., 1990) and torsion angle (Rice & Brünger, 1994) molecular dynamics were performed and the model with the lowest $R_{free}$ value was chosen for map calculation using DM (Cowtan, 1994), OMIT (Vellieux & Dijkstra, 1997), and the RAVE package (Kleywegt & Jones, 1994) for density modification prior to the next round of manual model building in O (Jones et al., 1991). Following the identification and addition of all deletions and insertions to the model, an attempt was made to include the higher resolution data. These reflections turned out to be of poor quality in dataset 1, due to ice formation during measurement, leading to unreasonably high *B*-factors and *R*-values that could not be improved further. Therefore, the final rounds of refinement were done with dataset 2 using the maximum-likelihood target function in REFMAC (Murshudov et al., 1997) and applying a bulk solvent model from X-PLOR (Jiang & Brünger, 1994). NCS restraints were lifted and water molecules were added to the model with the ARP software (Lamzin & Wilson, 1993) until $R_{free}$ stopped decreasing. The three N-terminal residues of both chains plus the C-terminal amino acid of monomer A were not visible in the electron density. The final model consists of 825 amino acid residues, 2 cofactor, and 118 water molecules. Refinement statistics are summarized in Table 2.

### *Docking calculations*

Prior to the simulation all water molecules where removed from the refined *T. cruzi* TAT structure model. Polar hydrogen atoms where added with HBPLUS (McDonald & Thornton, 1994), charges and radii where assigned using an adapted PARSE dataset (Sitkoff et al., 1994) in GRASP (Nicholls et al., 1991). The cofactor was charged using formal values (N1, +1; O3, −1; OP1-3, −0.667) under the assumption that the internal aldimine is unprotonated. The charges of the zwitterionic amino acid substrates were calculated with the MINDO/3 method (Baird & Dewar, 1969). Docking calculations were performed with AUTODOCK 2.4 (Morris et al., 1996), using a grid spacing of 0.2 Å around the cofactor of monomer A. A starting temperature of 1,500 K was chosen and 3,000 accepted plus 3,000 rejected steps were performed per temperature reduction cycle. For each amino acid 100 docking runs were carried out.

**Table 2.** *Refinement statistics*

| | |
|---|---|
| Resolution range | 10.0–2.51 Å (dataset 2) |
| $R$[a] | |
| Overall (%) | 15.7 |
| Last shell (%) | 21.1 (2.60–2.51 Å) |
| $R_{free}$ (5% of all reflections) | |
| Overall (%) | 21.4 |
| Last shell (%) | 29.4 (2.60–2.51 Å) |
| No. | |
| Protein and cofactor atoms | 6,472 |
| Water molecules | 118 |
| Average *B*-factor | |
| Protein and cofactor atoms (Å$^2$) | 25.2 |
| Water molecules (Å$^2$) | 25.0 |
| Residues in Ramachandran core region (%)[b] | 91 |
| NCS RMS (Å)[c] | 0.513 |
| Coordinate error (Å)[d] | 0.312 |
| Bond distance RMSD (Å) (target value: 0.02) | 0.006 |
| Angle distance RMSD (Å) (target value: 0.04) | 0.023 |
| *B*-factor RMSD (Å$^2$) (target value: 2.0) | 0.721 |

[a] $R$-factor; $R = \sum|F_{obs}| - k\cdot|F_{calc}|/\sum|F_{obs}|$ ($k$: scale factor, $|F_{obs}| > 0\sigma$).

[b] Ramachandran plot calculated with PROCHECK (Laskowski et al., 1993).

[c] Value calculated with WHATCHECK (Hooft et al., 1996) for all protein atoms related by noncrystallographic symmetry (NCS).

[d] Diffraction-component precision index based on $R_{free}$ (Cruickshank, 1999).

### *Figures*

Molecule representations where prepared with MOLSCRIPT (Kraulis, 1991) and BOBSCRIPT (Esnouf, 1997), molecular surfaces where calculated in GRASP (Nicholls et al., 1991). The figures where rendered with POV-Ray™ after combination and optimization in GL_RENDER (L. Esser & J. Deisenhofer, unpubl. data). Figure 2 was edited with ESPript (Gouet et al., 1999) after construction of a structure based sequence alignment in BRAGI (Schomburg & Reichelt, 1988), which was corrected for insertions and deletions in secondary structure elements by visual inspection in O (Jones et al., 1991). Secondary structure was identified with DSSP (Kabsch & Sander, 1993).

### *Accession number*

Structure coordinates have been deposited in the PDB (Sussman et al., 1998) and assigned the accession number 1BW0.

## Acknowledgments

We are very grateful to Dr. Juan J. Cazzulo, from Instituto de Investigaciones Biotecnologicas, Universidad de General San Martin, Argentina, for supplying the *T. cruzi* parasites, to Berta Franke de Cazzulo for the cell cultures, and to Sabine Weissflog for technical help with the crystallization experiments. Part of this work was supported by a grant from Universidad de Buenos Aires, and a joint grant from SECYT-CONICET, Argentina, and WTZ, BMBF, Bonn, Germany.

## References

Alexander FM, Sandmeier E, Mehta PK, Christen, P. 1994. Evolutionary relationships among pyridoxal-5′-phosphate-dependent enzymes. *Eur J Biochem 219*:953–960.

Andersson SM, Pispa JP. 1982. Purification and properties of human liver tyrosine aminotransferase. *Clin Chim Acta 125*:117–123.

Baird NC, Dewar MJS. 1969. Ground state of sigma-bonded molecules. IV. M.I.N.D.O. method and its applications to hydrocarbons. *J Chem Phys 50*:1262–1274.

Berger BJ, Dai WW, Wang H, Stark RE Cerami A. 1996. Aromatic amino acid transamination and methionine recycling in trypanosomatids. *Proc Natl Acad Sci USA 93*:4126–4130.

Berger BJ, Dai WW, Wilson J. 1998. Methionine formation from α-ketomethiobutyrate in the trypanosomatid *Crithidia fasciculata*. *FEMS Microbiol Lett 165*:305–312.

Biosym/MSI. 1996. *Crystallography workbench users guide*. San Diego, Califfornia: Biosym/MSI.

Bontempi EJ, Bua J, Aslund L, Porcel B, Segura EL, Henriksson J, Orn A, Pettersson U, Ruiz AM. 1993. Isolation and characterization of a gene from *Trypanosoma cruzi* encoding a 46-kilodalton protein with homology to human and rat tyrosine aminotransferase. *Mol Biochem Parasitol 59*:253–262.

Brünger AT. 1992. *X-PLOR, version 3.1: A system for X-ray crystallography and NMR.* New Haven, Connecticut: Yale University Press.

Brünger AT, Krukowski A, Erickson J. 1990. Slow-cooling protocols for crystallographic refinement by simulated annealing. *Acta Cryst A46*:585–593.

Cazzulo JJ. 1992. Energy metabolism in *Trypanosoma cruzi*. *Subcell Biochem 18*:235–57.

Cazzulo JJ, Franke de Cazzulo BM, Engel JC, Cannata JJB. 1985. End products and enzyme levels of aerobic glucose fermentation in Trypanosomatids. *Mol Biochem Parasitol 16*:329–343.

CCP4 (Collaborative Computational Project No. 4). 1994. The CCP4 suite: Programs for protein crystallography. *Acta Crystallogr D50:*760–763.

Chatterjee AN, Ghosh JJ. 1957. Transaminases of *Leishmania donovani*, the causative agent of Kala azar. *Nature 180*:1425.

Constansas NS, Levis GM, Vakirtzi-Lemonias CS. 1971. *Crithidia fasciculata* tyrosine aminotransferase. Characterization and differentiation from alanine aminotransferase. *Biochim Biophys Acta 230*:137–145.

Cowtan KD. 1994. "dm": An automated procedure for phase improvement by density modification. *Joint CCP4 and ESF-EACBM Newsletter on Protein Crystallography 31*:34–38.

Cruickshank DWJ. 1999. Remarks about protein structure precision. *Acta Crystallogr D55:*583–601.

Dietrich JB, Lorber B, Kern D. 1991. Expression of mammalian tyrosine aminotransferase in *Saccharomyces cerevisiae* and *Escherichia coli*. Purification to homogeneity and characterization of the enzyme overproduced in the bacteria. *Eur J Biochem 201*:399–407.

El Sawalhy A, El-Sherbini S. 1997. Diagnosis of chronic camel trypanosomosis by detection of the antibody of trypanosome tyrosine aminotransferase. *Dtsch tierärztl Wschr 104*:531–533.

El Sawalhy A, Seed JR, Hall JE, El Attar H. 1998. Increased excretion of aromatic amino acids catabolites in mammals infected with *Trypanosoma brucei evansi*. *J Parasitol 84*:469–473.

Esnouf RM. 1997. An extensively modified version of MolScript that includes greatly enhanced coloring capabilities. *J Mol Graph Model 15*:112–113, 132–134.

Evans P. 1997. Scala. *CCP4 and ESF-EACBM Newsletter on Protein Crystallography 33*:22–24.

Fair DS, Krassner SM. 1971. Alanine aminotransferase and aspartate aminotransferase in *Leishmania tarentolae*. *J Parasitol 18*:441–444.

Fellman JH, Vanbellinghen PJ, Jones RT, Koler RD. 1969. Soluble and mitochondrial forms of tyrosine aminotransferase: Relationship to human tyrosinemia. *Biochemistry 8*:615–622.

Flohé L. 1998. The Achilles' heel of trypanosomatids: Trypanothione-mediated hydroperoxide metabolism. *Biofactors 8*:87–91.

Ford GC, Eichele G, Jansonius JN. 1980. Three-dimensional structure of a pyridoxal-phosphate-dependent enzyme, mitochondrial aspartate aminotransferase. *Proc Natl Acad Sci USA 77*:2559–2263.

Gouet P, Courcelle E, Stuart DI, Metoz F. 1999. SPript: Analysis of multiple sequence alignments in PostScript. *Bioinformatics 15*:305–308.

Grange T, Pictet R. 1985. Complete complementary DNA of rat tyrosine aminotransferase messenger RNA. Deduction of the primary structure of the enzyme. *J Mol Biol 184*:347–350.

Hanhart E. 1947. Neue Sonderformen von Keratosis palmo-plantaris, u.a. eine regelmäßig-dominante mit systematisierten Lipomen, ferner 2 einfach-rezessive mit Schwachsinn und z.T. mit Hornhautveränderungen des Auges (Ektodermatosyndrom). *Dermatologica 94:*286–308.

Hargrove JL. 1988. Persulfide generated from L-cysteine inactivates tyrosine aminotransferase. Requirement for a protein with cysteine oxidase activity and γ-cystathionase. *J Biol Chem 263*:17262–17269.

Hargrove JL, Wichman RD. 1987. A cystine-dependent inactivator of tyrosine aminotransferase co-purifies with gamma-cystathionase (cystine desulfurase). *J Biol Chem 262*:7351–7357.

Hayashi H, Mizuguchi H, Kagamiyama H. 1998. The imine-pyridine torsion of the pyridoxal 5′-phosphate Schiff base of aspartate aminotransferase lowers its p$K_a$ in the unliganded enzyme and is crucial for the successive increase in the p$K_a$ during catalysis. *Biochemistry 37*:15076–15085.

Hester G, Stark W, Moser M, Kallen J, Markovic-Housley Z, Jansonius JN. 1999. Crystal structure of phosphoserine aminotransferase from *Escherichia coli* at 2.3 Å resolution: Comparison of the unligated enzyme and a complex with α-methyl-L-glutamate. *J Mol Biol 286*:829–850.

Hooft RWW, Vriend G, Sander C, Abola EE. 1996. WHAT_CHECK (verification routines from WHAT IF): Errors in protein structures. *Nature 381*:272.

Hühn R, Stoermer H, Klingele B, Bausch E, Fois A, Farnetani M, Di Rocco M, Boue J, Kirk JM, Coleman R, Scherer G. 1998. Novel and recurrent tyrosine aminotransferase gene mutations in tyrosinemia type II. *Hum Genet 102*:305–313.

Hunziker N. 1980. Richner–Hanhart syndrome and tyrosinemia type II. *Dermatologica 160*:180–189.

Iwasaki Y, Lamar C, Danenberg K, Pitot HC. 1973. Studies on the induction and repression of enzymes in rat liver. Characterization and metabolic regulation of multiple forms of tyrosine aminotransferase. *Eur J Biochem 34*:347–357.

Jensen RA, Gu W. 1996. Evolutionary recruitment of biochemically specialized subdivisions of family I within the protein superfamily of aminotransferases. *J Bacteriol 178*:2161–2171.

Jiang JS, Brünger AT. 1994. Protein hydration observed by X-ray diffraction: Solvation properties of penicillopepsion and neuraminidase crystal structures. *J Mol Biol 243*:100–115.

Jones TA, Zou JY, Cowan SW, Kjeldgaard M. 1991. Improved methods for building protein models in electron density maps and the location of errors in these models. *Acta Crystallogr A47*:110–119.

Kabsch W, Sander C. 1993. Dictionary of protein secondary structure: Pattern recognition of hydrogen-bonded and geometrical features. *Biopolymers 22*:2577–2637.

Kirsch JF, Eichele G, Ford GC, Vincent MG, Jansonius JN, Gehring H, Christen P. 1984. Mechanism of action of aspartate aminotransferase proposed on the basis of its spatial structure. *J Mol Biol 174*:497–525.

Kleywegt GJ, Jones TA. 1994. Halloween . . . masks and bones. In: *From first map to final model*. Warrington, UK: SERC Daresbury Laboratory. pp 59–66.

Kraulis P. 1991. A program to produce both detailed and schematic plots of protein structures. *J Appl Crystallogr 24*:946–950.

Kuramitsu S, Hiromi K, Hayashi H, Morino Y, Kagamiyama H. 1990. Pre-steady-state kinetics of *Escherichia coli* aspartate aminotransferase catalyzed reactions and thermodynamic aspects of its substrate specificity. *Biochemistry 29*:5469–5476.

Lamzin VS, Wilson KS. 1993. Automated refinement of protein models. *Acta Crystallogr D49*:129–147.

Laskowski RA, MacArthur MW, Moss DS, Thornton JM. 1993. Procheck: A program to check the stereochemical quality of protein structures. *J Appl Crystallogr 26*:283–291.

Le Blanq SM, Lanham SM. 1984. Aspartate aminotransferase in *Leishmania* is a broad spectrum transaminase. *Trans Roy Soc Trop Med Hyg 78*:373–375.

Malashkevich VN, Onuffer JJ, Kirsch JF, Jansonius JN. 1995a. Alternating arginine-modulated substrate specificity in an engineered tyrosine aminotransferase. *Nat Struct Biol 2*:548–553.

Malashkevich VN, Strokopytov BV, Borisov VV, Dauter Z, Wilson KS, Torchinsky YM. 1995b. Crystal structure of the closed form of chicken cytosolic aspartate aminotransferase at 1.9 Å resolution. *J Mol Biol 247*:111-124.

McDonald IK, Thornton JM. 1994. Satisfying hydrogen bonding potential in proteins. *J Mol Biol 238*:777–793.

McPhalen CA, Vincent MG, Picot D, Jansonius JN, Lesk AM, Chothia C. 1992. Domain closure in mitochondrial aspartate aminotransferase. *J Mol Biol 227*:197–213.

Mehta PK, Hale TI, Christen P. 1993. Aminotransferases: Demonstration of homology and division into evolutionary groups. *Eur J Biochem 214*:549–561.

Miller JE, Litwack G. 1971. Purification, properties and identity of liver mitochondrial tyrosine aminotransferase. *J Biol Chem 246*:3234–3240.

Montemartini M, Santomé JA, Cazzulo JJ, Nowicki C. 1993. Purification and parial structural and kinetic characterization of tyrosine aminotransferase from epimastigotes of *Trypanosoma cruzi*. *Biochem J 292*:901–906.

Montemartini M, Santomé JA, Cazzulo JJ, Nowicki C. 1994a. Production of aromatic α-hydroxy acids by epimastigotes of *Trypanosoma cruzi*, and its possible role in NADH re-oxidation. *FEMS Microbiol Lett 118*:89–92.

Montemartini M, Santomé JA, Cazzulo JJ, Nowicki C. 1994b. Purification and partial structural and kinetic characterization of an aromatic L-α-hydroxy acid dehydrogenase from epimastigotes of *Trypanosoma cruzi*. *Mol Biochem Parasitol 68*:15–23.

Morris GM, Goodsell DS, Huey R, Olson AJ. 1996. Distributed automated docking of flexible ligands to proteins: Parallel applications of AutoDock 2.4. *J Comput Aided Mol Des 10*:293–304.

Murshudov GN, Vagin AA, Dodson EJ. 1997. Refinement of macromolecular structures by the maximum-likelihood method. *Acta Crystallogr D53*:240–255.

Natt E, Kida K, Odievre M, Di Rocco M, Scherer G. 1992. Point mutations in the tyrosine aminotransferase gene in tyrosinemia type II. *Proc Natl Acad Sci USA 89*:9297–9301.

Navaza J. 1994. An automated package for molecular replacement. *Acta Crystallogr A50*:157–163.

Nicholls A, Sharp KA, Honig B. 1991. Protein folding and association: Insights from the interfacial and thermodynamic properties of hydrocarbons. *Proteins 11*:281–296.

Nogoceke E, Gommel DU, Kieß M, Kalisz HM, Flohé L. 1997. A unique cascade of oxidoreductases catalyzes trypanothione-mediated peroxide metabolism in *Crithidia fasciculata*. *Biol Chem 378*:827–836.

Nowicki C, Montemartini M, Duschak V, Santome JA, Cazzulo JJ. 1992. Presence and subcellular localization of tyrosine aminotransferase and p-hydroxyphenyllactate dehydrogenase in epimastigotes of *Trypanosoma cruzi*. *FEMS Microbiol Lett 71*:119–124.

Nowicki C, Montemartini M, Hunter GR, Blankenfeldt W, Kalisz HM, Hecht HJ. 1998. Crystallization and preliminary X-ray analysis of tyrosine aminotransferase from *Trypanosoma cruzi* epimastigotes. *Acta Crystallogr D54*:105–107.

Okamoto A, Higuchi T, Hirotsu K, Kuramitsu S, Kagamiyama H. 1994. X-ray crystallographic study of pyridoxal 5′-phosphate-type aspartate aminotransferases from *Escherichia coli* in open and closed form. *J Biochem 116*:95–107.

Okamoto A, Nakai Y, Hayashi H, Hirotsu K, Kagamiyama H. 1998. Crystal structures of *Paracoccus denitrificans* aromatic amino acid aminotransferase: A substrate recognition site constructed by rearrangement of hydrogen bond network. *J Mol Biol 280*:443–461.

Opperdoes FR. 1987. Compartmentation of carbohydrate metabolism in trypanosomes. *Annu Rev Microbiol 41*:127–151.

Otwinowski Z. 1993. Data collection and processing. In: *CCP4 Daresbury study weekend*. Warrington, UK: SERC Daresbury Laboratory.

Rege AA. 1987. Purification and characterization of a tyrosine aminotransferase from *Crithidia fasciculata*. *Mol Biochem Parasitol 25*:1–9.

Rettenmeier R, Natt E, Zentgraf H, Scherer G. 1990. Isolation and characterization of the human tyrosine aminotransferase gene. *Nucleic Acids Res 18*:3853–3861.

Rhee S, Silva MM, Hyde CC, Rogers PH, Metzler CM, Metzler DE, Arnone A. 1997. Refinement and comparisons of the crystal structures of pig cytosolic aspartate aminotransferase and its complex with 2-methylaspartate. *J Biol Chem 272*:17293–17302.

Rice LM, Brünger AT. 1994. Torsion angle dynamics: Reduced variable conformational sampling enhances crystallographic structure refinement. *Proteins 19*:277–290.

Richner H. 1938. Hornhautaffektion bei Keratoma palmare et plantare hereditarium. *Klin Mbl Augenheilk 100*:580–588.

Schomburg D, Reichelt J. 1988. BRAGI: A comprehensive protein modeling program system. *J Mol Graphics 6*:161–165.

Sitkoff D, Sharp KA, Honig B. 1994. Correlating solvation free energies and surface tensions of hydrocarbon solutes. *Biophys Chem 51*:397–403.

Stibbs HH, Seed JR. 1975a. Metabolism of tyrosine and phenylalanine in *Trypanosoma brucei gambiense*. *Int J Biochem 6*:197–203.

Stibbs HH, Seed JR. 1975b. Short-term metabolism of 14C tryptophan in rats infected with *Trypanosoma brucei gambiense*. *J Infect Dis 131*:459–462.

Sussman JL, Lin D, Jiang J, Manning NO, Prilusky J, Ritter O, Abola EE. 1998. Protein Data Bank (PDB): Database of three-dimensional structural information of biological macromolecules. *Acta Crystallogr D54*:1078–1084.

Tong L, Rossmann MG. 1990. The locked rotation function. *Acta Crystallogr A46*:783–792.

Vellieux FMD, Dijkstra BW. 1997. Computation of Bhat's OMIT maps with different coefficients. *J Appl Crystallogr 30*:396–399.

Vernal J, Cazzulo JJ, Nowicki C. 1998. Isolation and partial characterization of a broad specificity aminotransferase from *Leishmania mexicana* promastigotes. *Mol Biochem Parasitol 96*:83–92.

World Health Organisation. 1998. *The World Health Report 1998. Life in the 21st century: A vision for all*. Geneva, Switzerland: World Health Organisation.

Yano T, Kuramitsu S, Tanase S, Morino Y, Kagamiyama H. 1992. Role of Asp222 in the catalytic mechanism of *Escherichia coli* aspartate aminotransferase: The amino acid residue which enhances the function of the enzyme-bound coenzyme pyridoxal 5′-phosphate. *Biochemistry 31*:5878–5887.